ACS APPLIED MATERIALS & INTERFACES

Research Article

www.acsami.org

Synergistic Hybrid Organic–Inorganic Aerogels

Xiao Wang and Sadhan C. Jana*

Department of Polymer Engineering, The University of Akron, Akron, Ohio 44325, United States

ABSTRACT: A class of inorganic–organic hybrid mesoporous aerogel structure was synthesized by growing gel in a gel. In Type 1, silica gels were grown inside the macropores of thermoreversible syndiotactic polystyrene (sPS) gel, while Type 2 hybrid aerogels were obtained by thermoreversible gelation of sPS chains in the mesopores of preformed silica gel. The hybrid gels were converted into aerogels by exchanging the solvent with liquid carbon dioxide followed by supercritical drying. The hybrid aerogels presented cocontinuous networks of pearl-necklace silica particles and crystalline strands of sPS and exhibited the "petal effect" due to the presence of superhydrophobic sPS and hygroscopic silica. The compressive modulus and compressive strain show large enhancements over sPS and silica aerogels indicating synergy, although Type 1 hybrid aerogels were found to be more robust. The hybrid aerogels showed fast absorption and high absorption capacity for a representative hydrocarbon liquid.

KEYWORDS: *syndiotactic polystyrene aerogel, silica aerogel, hybrid, synergy, surface property*

1. INTRODUCTION

Aerogels are a unique class of open-celled, highly porous, solid state materials composed of interconnected nanostructures filled with air. The solid networks of aerogels are first synthesized in the form of gels, and the liquid in the gel is extracted under supercritical condition so that the solid networks do not collapse.[1,2]

Silica aerogels are the most widely studied aerogel material system for their exclusive properties and versatile chemistry. The most intriguing properties for silica aerogels include extremely large surface area (ca. 1000 m^2/g), low thermal conductivity (0.004 to 0.03 W/m·K), low dielectric constant (1.1–2.2), and low index of refraction (~1.05), leading their niche applications in thermal insulation, high energy physics, molecular separation, to name a few.[3−9] However, the inherent fragility and hygroscopic nature somewhat restrict their applications. The fragility of silica aerogels is more prominent for "pearl necklace" microstructures held together by a limited number of Si–O–Si bonds at the "neck" of secondary silica particles.[10] A native silica aerogel derived from tetramethoxysilane (TMOS) with a density of 0.12 g/mL can be completely crushed into dust under a small stress of 31 kPa.[11]

For silica aerogels conventionally dried using supercritical carbon dioxide, the residual Si–OH bonds on surfaces of silica particles are responsible for their hygroscopic nature. A drop of water placed on silica aerogels can easily destroy the aerogel network.[12,13] In this case, water sucked into mesopores develops large capillary force, which in turn exerts a stress component squeezing the particles and leading to failure. Effective reinforcement of silica aerogels calls for strategies such as conformal coating of polymer on the silica backbone,[14−16] strengthening the neck region using polymer chain or multifunctional nanoparticles,[17−20] reinforcing the network with nanofibers,[21−23] and treatment with silylating agent such as chlorotrimethylsilane.[24,25] The polymer- and nanoparticle-reinforced aerogels also exhibit hydrophobicity due to incorporation of organic groups and polymer chains. However, the modification methods also brought about new issues such as substantially higher density, a large reduction of surface area, and loss of clarity.

Syndiotactic polystyrene (sPS) aerogels have also received considerable attention since the first report by Daniel et al. in 2005.[26] In contrast to silica aerogels, the intermolecular physical bonding of the chains in the crystalline junctions holds together the three-dimensional networks in sPS aerogels. sPS aerogels offer a combination of macropores (diameter > 50 nm) formed between the adjoining strands of sPS and micropores (diameter < 2 nm) formed inside the individual crystalline strands. sPS aerogels show fast sorption kinetics[27,28] and can absorb and imprison guest molecules, such as volatile

Received: May 8, 2013
Accepted: June 17, 2013
Published: June 17, 2013

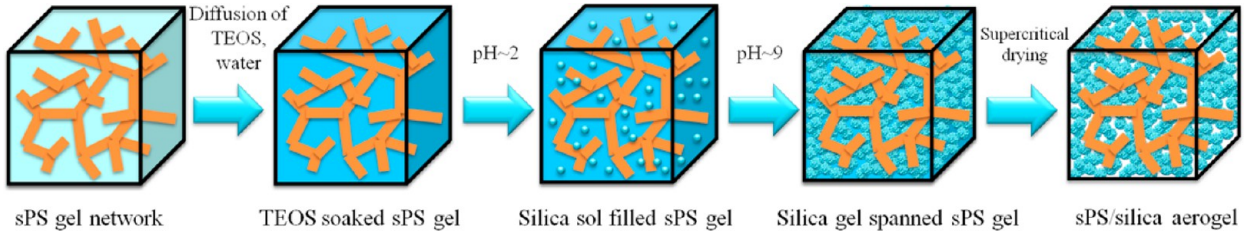

Figure 1. Schematic illustration of Type 1 sPS/silica hybrid aerogel preparation procedure.

organic compounds, into crystalline nanocavities with an apparent increase in guest molecule diffusivity of up to 7 orders of magnitude with respect to sPS films.[29] sPS aerogels do not shatter easily like silica aerogels, but undergo irreversible network strand buckling under small stress.[30] sPS chains exhibit strong chemical inertness for its crystalline structures and thus lack flexibility for chemical modification.

In this work, a new mesoporous hybrid aerogel was obtained by combining sPS and silica aerogels into a single structure. The new hybrid aerogel offers the following attributes: (i) the nanocavities of sPS crystalline strands can be used for absorption of volatile organic compounds, (ii) the macropores of sPS and silica aerogel can account for large volume uptake of organic polar and nonpolar liquids and water, (iii) the mesopores of silica can screen different size particles or deformable droplets, and (iv) far superior mechanical properties can be achieved over sPS and silica aerogels. To the best of our knowledge, this is the first example where organic and inorganic aerogels are synergistically combined.

The synergistic effects in this new class of materials are derived as follows. First, the rigid silica particles support sPS strands against buckling at a low compressive stress. Second, the neighboring sPS strands cage the silica particle networks and prevent their fracture under compression. Third, the superhydrophobic sPS networks prevent complete wetting of the material by water and circumvent spontaneous fracture of the silica aerogel part when exposed to water droplets. Fourth, the mesoporous silica aerogels offer much higher intrinsic surface area compared to sPS aerogels.

2. EXPERIMENTAL SECTION

2.1. Materials. Syndiotactic polystyrene (molecular weight of 300 000 g/g mol, density 1.05 g/mL) in the form of pellets was purchased from Scientific Polymer Products Inc. (Ontario, NY). The sPS pellets were grinded into powder for easy dissolution in solvents. Tetraethylorthosilicate (TEOS, reagent grade, 98%), nitric acid (purity, 64−66%), and ammonium hydroxide solution (28−30%, NH_3 basis) were purchased from Sigma Aldrich and used as received. Reagent grade tetrahydrofuran (THF) and ethanol were purchased from Fisher Scientific and used without further purification.

2.2. Preparation of sPS/Silica Hybrid Aerogels. One cannot simply mix the two gel precursor materials together to obtain a hybrid sPS/silica aerogel, as the mechanisms of silica and sPS gel formation are quite different. In view of this, a two-step method was used in this work. This involved preparation of one gel network first followed by an in situ growth of the second gel network inside the first gel. This provided two types of hybrid aerogels. In Type 1, the sPS gel was prepared first using typical thermoreversible gelation procedure. The silica gel was then grown inside the sPS gel network following an acid−base catalyzed sol−gel process. In Type 2, the silica gel network was first synthesized and sPS chains were allowed to form a gel inside the silica gel by thermoreversible gelation. This paper discusses the results involving both Type 1 and Type 2 hybrid aerogels.

For synthesis of Type 1 hybrid aerogels, sPS powder was added into THF and the mixture was heated to 160 °C in a sealed vial until dissolution of the solids was complete. The solution was then transferred to a cylindrical mold and allowed to stand for 24 h at room temperature for gelation. THF in sPS gel was exchanged with ethanol by washing the gel approximately every 4 h for a total of 5 times, resulting in sPS alcogel. The growth of silica gel within sPS gel network was then conducted by an acid−base catalyzed sol−gel process. The sPS alcogel was immersed in a solution containing TEOS (20.8 g), deionized water (5.4 g), and ethanol (40 mL) overnight, allowing TEOS and water to diffuse inside the sPS gel. Subsequently, TEOS was partially hydrolyzed by using nitric acid and the pH of the solution was adjusted to a value of 2. The sPS alcogel soaked with partially hydrolyzed TEOS was transferred to another solution containing ammonium hydroxide (0.5 mL), deionized water (7.2 g), and ethanol (30 mL) and condensation of silica sol into gel occurred. The gel was allowed to stand in the solution for 24 h. The resultant hybrid gel was washed with ethanol five times to remove the residual water. These hybrid gels were synthesized using three concentrations of sPS and a fixed concentration of TEOS. The solvent ethanol was removed from the gel by liquid carbon dioxide. The gel was then dried under supercritical condition of carbon dioxide. For this purpose, the wet gel was placed in an autoclave and liquid CO_2 was fed into the autoclave. The gel was soaked in liquid CO_2 for 2 h, followed by drainage of the solvent and refilling. The soaking and washing steps were repeated five times, and the vessel was heated to 50 °C and kept at 11.5 MPa pressure for 1 h, which is above the critical point of CO_2 (31 °C, 7.4 MPa).[2] The vessel was depressurized at 50 °C for venting of CO_2 under supercritical condition. Residual solvent was removed by keeping the specimens overnight in a vacuum oven. The corresponding hybrid aerogel samples are denoted as "sPS- wt g/mL-silica" in the rest of the paper. The structural changes during hybrid aerogel preparation are shown schematically in Figure 1.

For Type 2 hybrid aerogels, silica gel was first prepared using acid−base catalyzed gelation scheme described above. Water in silica gel was exchanged with ethanol by washing the gel approximately every 4 h for a total of five times followed by exchange of ethanol with THF using the same procedure. The resultant silica gel was immersed in a solution of sPS/THF (0.05 g/mL) at 110 °C in a sealed vial for 6 h to allow diffusion of sPS into silica gel. The warm silica gel was then transferred into cold THF first to wash out the sPS chains adhering to the surfaces of the gel and second to allow thermoreversible gelation of sPS inside the silica gel. The Type 2 hybrid aerogels were recovered by exchanging THF with liquid carbon dioxide and by supercritical drying.

2.3. Characterization. The bulk density ρ_b of aerogels was obtained from the weight and volume of the cylindrical specimens. The skeletal density ρ_s was measured using an Accupyc 1340 helium pycnometer (Micrometrics Instrument Corp). The skeletal density can be used in conjunction with the bulk density to calculate porosity p. The diameter shrinkage δ_d was determined from the difference of diameter of the aerogel and the corresponding gel specimen. The bulk density (ρ_b), porosity (p), and diameter shrinkage (δ_d) of the aerogels were calculated using the following relationships:

$$\rho_b = \frac{4m}{\pi D^2 h} \quad (1)$$

dx.doi.org/10.1021/am401717s | ACS Appl. Mater. Interfaces 2013, 5, 6423−6429

Table 1. Composition and Properties of Type 1 Hybrid Aerogels[a]

sample name	shrinkage (%)	bulk density (g/mL)	skeletal density (g/mL)	porosity (%)	surface area (m^2/g)	compressive modulus (MPa)	m_s/m_p	V_s/V_p
sPS-0.02	11 ± 0.5	0.032 ± 0.0004	1.056 ± 0.0022	97.0	379	1.7 ± 0.04	N/A	N/A
sPS-0.02-silica	5 ± 0.1	0.117 ± 0.0006	1.586 ± 0.0029	92.6	736	4.5 ± 0.55	4.20	2.47
sPS-0.04	7 ± 0.7	0.056 ± 0.0014	1.056 ± 0.0022	94.7	377	6.1 ± 0.62	N/A	N/A
sPS-0.04-silica	6 ± 1.2	0.146 ± 0.0059	1.443 ± 0.0009	89.9	651	11.5 ± 0.22	1.84	1.08
sPS-0.08	6 ± 0.1	0.102 ± 0.0005	1.056 ± 0.0022	90.3	377	19.5 ± 2.77	N/A	N/A
sPS-0.08-silica	5 ± 0.1	0.181 ± 0.0011	1.326 ± 0.0007	86.3	540	24.5 ± 1.97	0.97	0.57
Silica	7 ± 0.2	0.118 ± 0.0036	1.801 ± 0.0108	93.4	1015	0.8 ± 0.18	N/A	N/A

[a]The quantities m_s/m_p and V_s/V_p indicate, respectively, the weight ratio and volume ratio of silica over sPS in the hybrid aerogel.

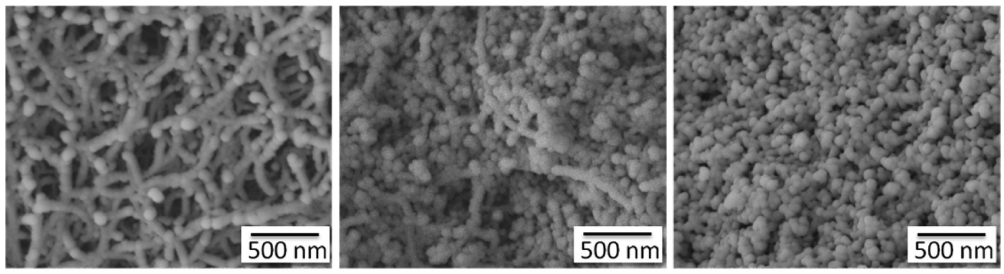

(a) sPS-0.02 Porosity: 97% (b) sPS-0.02-Silica Porosity: 92.6% (c) Silica Porosity: 93.4%

Figure 2. SEM images of (a) sPS aerogel, (b) Type 1 hybrid aerogel, and (c) silica aerogel.

$$p = \left(1 - \frac{\rho_b}{\rho_s}\right) \times 100 \quad (2)$$

$$\delta_d = 1 - \frac{D}{D_0} \quad (3)$$

In eqs 1−3, m is the weight of the aerogel, D and h are, respectively, the diameter and height of the cylindrical specimen, and D_0 is the diameter of the gel.

The morphology of aerogels was observed using scanning electron microscopy (SEM; JEOL JSM5310) with operating voltage 8 kV. For this purpose, the aerogels were fractured at room temperature and mounted on an aluminum stub using adhesive carbon tape and subsequently sputter-coated by a thin layer of silver particles under argon atmosphere using a sputter coater, model ISI 5400.

The thermal stability of samples under nitrogen atmosphere was investigated by thermogravimetric analysis (TGA). Approximately 5 mg of sample was placed in the platinum pan and heated from room temperature to 700 °C at a heating rate of 10 °C/min under nitrogen atmosphere using a TGA 2050 device (TA Instrument, New Castle, DE). The temperature at the onset of thermal degradation or 5% mass loss was estimated from a mass versus temperature plot.

The values of contact angle were measured using a Rame-Hart model 500 advanced goniometer equipped with a tilting base and automated dispensing system. In the static sessile drop method, a 5 μL drop of liquid was placed on the sample surface, and the image was captured and analyzed with ImageJ software. Five measurements were taken for each specimen to obtain reproducible data. For sample preparation, the aerogels were carefully fractured and the specimen with flat fractured surface was selected. In addition, the aerogel samples were compressed under a pressure of 3000 psi for 5 min to remove the pores and to obtain solid discs. The contact angle values on compressed discs were used to obtain information on surface energy and polarity of the polymeric materials without the interference from the pore structure. The contact angle values of both water and diiodomethane were measured. The value of total surface energy (γ), and the polar (γ^p) and dispersion (γ^d) components of total energy were calculated using eq 4 based on Wu's theory:[31]

$$\gamma_{LS} = \gamma_L + \gamma_S - \frac{4\gamma_L^d\gamma_S^d}{\gamma_L^d + \gamma_S^d} - \frac{4\gamma_L^p\gamma_S^p}{\gamma_L^p + \gamma_S^p} \quad (4)$$

In eq 4, γ_{LS} is the interfacial tension between liquid and solid, γ_L is the surface tension of the liquid, γ_S is the surface tension of the solid, and γ^d and γ^p are the dispersion (nonpolar) and polar components of surface tension, respectively. The values of surface energy γ^d = 21.8 dyn/cm and γ^p = 50.7 dyn/cm for water, γ^d = 44.1 dyn/cm and γ^p = 6.7 dyn/cm for diiodomethane were used in calculations.[31] The value of surface polarity was determined as the ratio of polar component of free energy to surface free energy, and calculated using eq 5:

$$\text{polarity} = \frac{\gamma_s^p}{\gamma_s^p + \gamma_s^d} \quad (5)$$

Brunauer−Emmett−Teller (BET) surface area and pore size distribution of aerogel specimens were obtained from nitrogen adsorption−desorption isotherms at 77 K, analyzed using a Micromeritics Tristar II 3020 analyzer. The aerogel specimens were sectioned and placed in designated chamber followed by degassing at room temperature for 12 h before collecting data. Data for adsorption and desorption isotherms were collected by using nitrogen as the adsorbent at 77 K. The surface area of the aerogels was calculated using BET method, and pore size distribution was calculated using Barrett−Joyner−Halenda (BJH) method.

The compressive properties of the aerogels were determined per ASTM D595 method using cylindrical specimens and Instron 5567 (Canton, MA) testing instrument. Rapid buckling occurred with standard specimens of sPS aerogel. This was avoided by using cylindrical aerogel specimens of diameter ∼11 mm and height-to-diameter ratio 1:1. The top and bottom surfaces of the aerogel specimens were polished to ensure good contact with the compression fixture. A crosshead speed of 1.27 mm/min was used and data for five specimens were collected to obtain average values of compressive strength, strain, and modulus.

3. RESULTS AND DISCUSSION

3.1. Type 1 Hybrid Aerogels. In Type 1 hybrid aerogel, the concentration of sPS in solution was varied from 0.02 to 0.08 g/mL and the concentration of silica was fixed in all

specimens at 1.0 mol/L. In Table 1, samples "sPS-0.02" and "sPS-0.02-silica" represent, respectively, sPS aerogel obtained with 0.02 g/mL solution of sPS and hybrid aerogel obtained with 0.02 g/mL solution of sPS and 1.0 mol/L of silica.

As seen in Table 1, the hybrid aerogel specimens exhibit lower shrinkage in diameter compared to both single material aerogels. This is more prominent at lower sPS concentration, for example, ~11% shrinkage for "sPS-0.02" aerogel compared to ~5% for the hybrid aerogel "sPS-0.02-silica". This can be attributed to rigid silica aerogel network preventing shrinkage of the weaker, low density sPS networks. Nevertheless, the additional weight of the silica particles in a fixed volume caused an increase of bulk density in hybrid aerogels over sPS aerogel. A comparison of the bulk density values in Table 1 indicates that the bulk density increase is approximately 0.08 g/mL for all hybrid aerogels. The values of skeletal density, however, are in between that of sPS aerogel and silica aerogel and depend on the concentration of sPS. All aerogel specimens listed in Table 1 show high values of porosity, although the porosity is slightly lower for hybrid aerogels due to higher bulk density.

SEM images in Figure 2 present evidence that sPS/silica hybrid aerogel networks were indeed formed using the procedure followed in this work. Figure 2 presents a qualitative, visual view of the following images: (a) macropores of sPS and (b) macropores of sPS network filled with mesoporous silica aerogel. The native sPS aerogels contain fiberlike network structures with strand diameter of 50−100 nm and macropores (diameter > 50 nm) formed by the sPS strands (Figure 2a). The micropores (diameter < 2 nm) located within the crystalline domains of sPS could not be identified in SEM images. The silica aerogels show a pearl-necklace structure (Figure 2c) with clustered particles of diameter 70−90 nm. The clustered particles also formed much smaller interstices known as mesopores of diameter between 2 and 50 nm. The hybrid aerogel shows a dual morphology of fiber strands of sPS and spherical particles of silica (Figure 2b). As sPS gel network was first created, the second network of silica particles could only form in the macropores of sPS networks. These images do not say anything about pore size distribution and the mean mesopore size.

The silica networks in hybrid aerogels are quantitatively identified in terms of mesopore size distribution presented in Figure 3. This figure confirms that silica networks contributed mesopores to the hybrid aerogel. The pore size distributions presented in Figure 3 indicate the following trends. First, the bulk-grown silica aerogel contained mesopores with a predominant pore size of approximately 9 nm. On the other hand, sPS aerogel did not contain predominant pores in the 2−50 nm range. All hybrid aerogels show predominant mesopores with the peak pore size greater than that of bulk-grown silica aerogel, for example, ~20 nm for sPS-0.02-silica, ~40 nm for sPS-0.04-silica, and ~30 nm for sPS-0.08-silica. These indicate that mesoporous silica gel grown inside the macropores of sPS gel contained larger pores. Thus, the growth and connectedness of silica particles in the confined macropores of sPS networks were hindered leading to larger silica mesopores in hybrid aerogels. At higher sPS concentrations, the morphology of hybrid aerogels did not show change in SEM images, although the mesopore size distribution became narrower (Figure 3). This is probably due to higher network density of sPS, guiding denser packing of silica particles in its macropores. This may also explain why the predominant mesopore size for sPS-0.08-silica aerogel was smaller than that of sPS-0.04-silica.

Silica aerogels upon heating in a thermogravimetric analyzer (TGA) exhibited a small weight loss (~2.5 wt %) at around 100 °C associated with removal of absorbed moisture by the hygroscopic aerogel (Figure 4a) and greater weight loss at 300

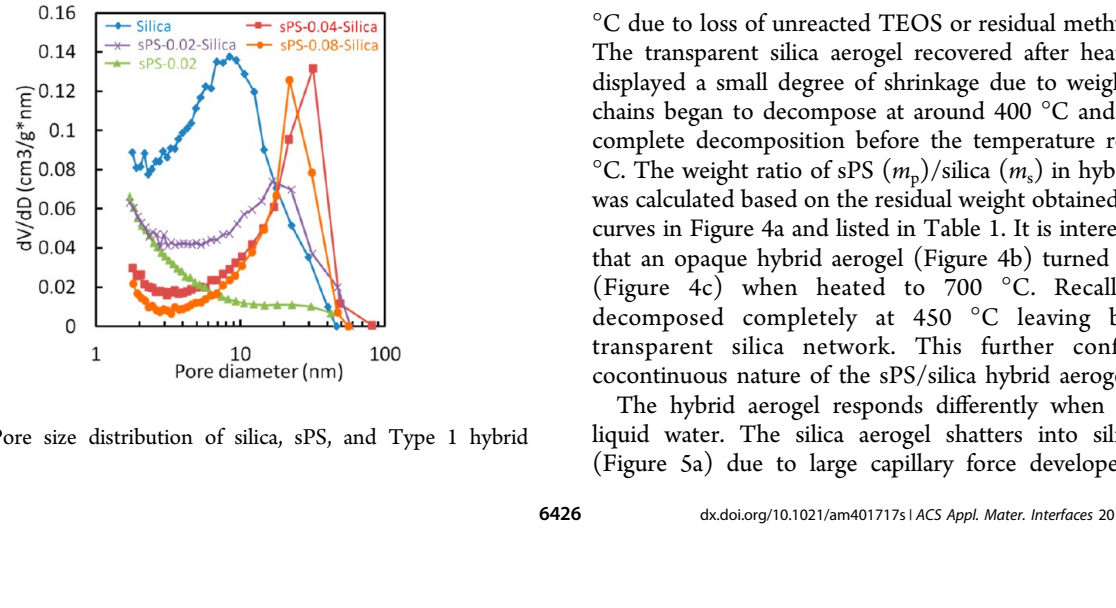

Figure 4. (a) TGA curves of Type 1 aerogel (20 °C/min, nitrogen atmosphere), and images of hybrid aerogel (b) before and (c) after heating to 700 °C in air.

Figure 3. Pore size distribution of silica, sPS, and Type 1 hybrid aerogels.

°C due to loss of unreacted TEOS or residual methyl groups.[32] The transparent silica aerogel recovered after heat treatment displayed a small degree of shrinkage due to weight loss. sPS chains began to decompose at around 400 °C and underwent complete decomposition before the temperature reached 450 °C. The weight ratio of sPS (m_p)/silica (m_s) in hybrid aerogels was calculated based on the residual weight obtained from TGA curves in Figure 4a and listed in Table 1. It is interesting to see that an opaque hybrid aerogel (Figure 4b) turned transparent (Figure 4c) when heated to 700 °C. Recall that sPS decomposed completely at 450 °C leaving behind the transparent silica network. This further confirmed the cocontinuous nature of the sPS/silica hybrid aerogel.

The hybrid aerogel responds differently when exposed to liquid water. The silica aerogel shatters into silica powder (Figure 5a) due to large capillary force developed as water

dx.doi.org/10.1021/am401717s | ACS Appl. Mater. Interfaces 2013, 5, 6423−6429

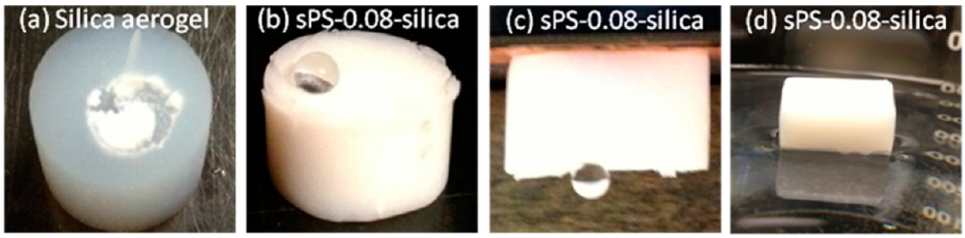

Figure 5. Images of Type 1 aerogels exposed to deionized water. (a) Water absorbed by silica aerogel, (b) water droplet sat on top of sPS/silica aerogel, (c) water droplet pinned to the aerogel surface when tilted upside down, and (d) a piece of sPS/silica aerogel floated on top of water.

permeates into the mesoporous structure.[12,13] In contrast, sPS aerogel is superhydrophobic. The hybrid aerogel system, however, offers high water contact angle, for example, 148°, for aerogel sPS-0.08-silica (Figure 5b) and shows pinning of the water droplet to the surface even when tilted upside down (Figure 5c). The hybrid aerogel sample sPS-0.08-silica can float on water for several days. This phenomenon is quite similar to the "petal effect" reported for sPS/PEO aerogel recently.[33] In the present case, the superhydrophobic sPS networks in hybrid aerogel contribute to high water contact angle and prevent wetting of the sample by water.

The polarity of the aerogel materials without the influence of porous structures was determined by measuring the contact angle on compressed aerogel samples as listed in Table 2. The polarity decreased substantially with an increase of sPS concentration and at higher sPS content, the polarity is quite close to that of sPS. Nevertheless, the presence of silica guarantees interactions with water and results in pinned water droplet seen in Figure 5c.

Table 2. Surface Polarity Data for Compressed Type 1 Aerogels Measured at 25 °C

	contact angle (deg)		
compressed aerogel	water	diiodomethane	polarity
silica	28	26	0.54
sps-0.02-silical	63	26	0.34
sps-0.04-silica	83	32	0.18
sps-0.08-silica	87	32	0.13
sps	89	36	0.12

The compressive stress–strain diagram in Figure 6 presents evidence of synergy in mechanical performance. It is noted that silica aerogels were inherently fragile and shattered at low stress at a strain of ~30%, while sPS aerogel did not shatter under small compressive load. However, sPS aerogel specimens experienced irreversible buckling at low stress and turned into dense solids at large compressive load. The hybrid aerogel did not shatter even at 70% strain. The compressive modulus was calculated from the slope of the initial linear portion of the stress–strain curves as shown in the inset of Figure 6a. The data of compressive modulus are plotted in Figure 6b. The compressive modulus of the hybrid aerogels is much higher than both silica and sPS aerogel. This unusual behavior can be interpreted in terms of how sPS strands and silica particles respond to compressive strain. The rigid silica particles provide support against buckling of sPS strands at low compressive stress, while the sPS networks lock the silica particles in tortuous macropores and prevent them from turning into dust under compressive stress. Multiwall carbon nanotubes produced similar reinforcement effects on sPS aerogels.[30]

The high surface area attributed to mesopores of silica and macro- and micropores of sPS was preserved in the hybrid aerogel structure as is evident from the data presented in Table 1. This poses a question of whether the cocontinuous sPS gel networks used in this work are any better in reinforcing silica aerogel than by cross-linking with polymers. Ilhan et al. proposed a three-dimensional core–shell structure where the core was the assembly of nanoparticles that comprised the skeletal framework of a typical silica aerogel, and the shell was polystyrene.[16] These authors reported high elastic modulus (30–60 MPa) and water contact angle around 120°. However, the surface area of aerogels reduced greatly to 213–393 m^2/g, and the density increased to as high as 0.41–0.77 g/mL. Nguyen et al. cross-linked silica aerogels containing an organic linking group, 1,6-bis(trimethoxysilyl)hexane (BTMSH) by polymerizing styrene.[19] They observed flexibility due to elastic contributions from BTMSH and improved strength owing to cross-linking by styrene. However, the materials offered high modulus (11–32 MPa) and also high bulk density (0.28–0.37

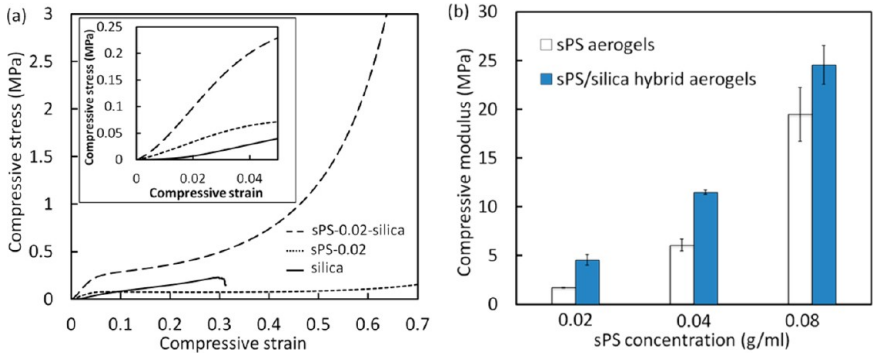

Figure 6. (a) Stress–strain curves for various Type 1 aerogels. The inset presents a close up of the linear regime at low strain. (b) Compressive modulus calculated from the slope of the initial linear portion of stress–strain curves.

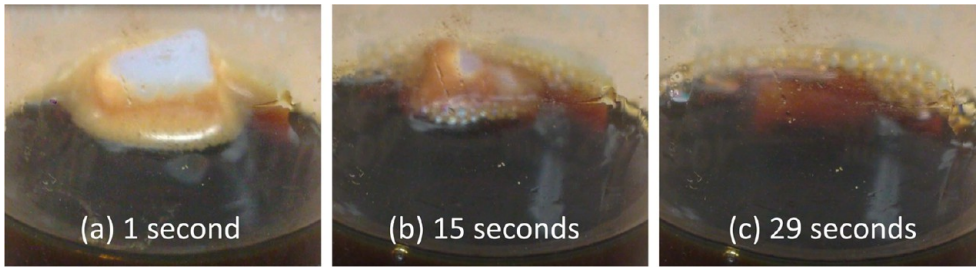

Figure 7. Images of sPS-0.02-silica Type 1 aerogel exposed to crude oil at different time: (a) 1 s, (b) 15 s, (c) 29 s.

g/mL). In the present work, the maximum bulk density for hybrid aerogel (sPS-0.08-silica) was 0.181 g/mL, while the compressive modulus was ~24 MPa.

We now turn to the results of a case study where the high surface area of the hybrid aerogels was exploited in absorbing a hydrocarbon liquid. The hybrid aerogel sPS-0.02-silica has a surface area 736 m^2/g, a porosity 92.6%, and an average pore size 14 nm (Table 1). This aerogel also showed fast absorption rate and high absorption capacity for crude oil, as seen in the snapshots taken from a video recording and presented in Figure 7. As soon as the hybrid aerogel was placed on top of the oil, plenty of fine air bubbles exited the aerogel. Simultaneously, the crude oil was rapidly absorbed by the aerogel. A 0.15 g specimen of sPS-0.02-silica aerogel submerged completely in oil within 30 s of exposure. The weight gain of the specimen was 6.07 g per gram of aerogel, which is close to the theoretical limit (6.34 g/g). The theoretical weight increase corresponds to a state when all pores are filled with the crude oil. For example, aerogel sPS-0.02-silica had a porosity of 92.6% and bulk density of 0.117 g/mL. If the aerogel with a physical volume V mL is used for crude oil absorption, the initial weight of the aerogel is $0.117V$ g and the volume of air in the aerogel is $0.926V$ mL. If all air in the aerogel is replaced with crude oil of density 0.801 g/mL, the maximum weight of crude oil is 0.801 g/mL × 0.926 mL × V or $0.742V$ g. Therefore, the theoretical weight of crude oil per gram of aerogel is $0.742V$ g/$0.117V$ g or 6.34 g/g. The theoretical crude oil uptake ratios of other aerogel specimens were computed in similar manner (Table 3). A very high theoretical uptake value of 24.29 for sPS-0.02 aerogel is due to its low (~0.03 g/cm^3) bulk density, which is about 1/4 the values of bulk density of hybrid aerogels.

Table 3. Crude Oil Absorption Data for Various Aerogels of Type 1[a]

	weight increase in g/gram of aerogel after				
sample name	0.5 min	1 min	5 min	equilibration time (min)	theoretical weight increase in g/gram of aerogel
sPS-0.02	6.02			0.5	24.29
sPS-0.02-silica	6.07			0.5	6.34
sPS-0.08	0.45	0.68	1.13	>60	7.09
silica	3.22	5.84		1	6.34

[a]The theoretical limit of weight increase is based on crude oil liquid density 0.801 g/mL.

The high absorption capacity and fast absorption rate can be attributed to two factors. First, the large capillary force induced by the mesopores promotes rapid intake of the oil into the highly porous aerogel. Second, the nanoporous, nonpolar sPS component of the hybrid aerogel produces fast absorption kinetics. Also note that the hybrid aerogel can float on water in a water−oil mixture, while the silica aerogel immediately disintegrates and sinks to the bottom of water. The sPS-0.02 aerogel presents another unique scenario. This material also shows fast absorption rate as the hybrid aerogel, but cannot reach a theoretical equilibrium absorption level of 24.29 g/g of aerogels. In this case, low network strength causes the network to collapse and the aerogel to shrink during oil absorption. Stronger and higher density sPS aerogel averts such network collapse, but the absorption kinetics is slow, as seen from the data presented in Table 3. The native silica aerogel with similar dimensions requires almost twice as long absorption time compared to a hybrid aerogel.

3.2. Type 2 Hybrid Aerogels. The morphology of Type 2 hybrid aerogel (Figure 8) is similar to that of Type 1 hybrid aerogel networks. Recall that sPS was allowed in this case to form a gel inside the preformed silica gel networks. The initially formed spherical silica particles and sPS fibrillar strands are clearly seen in the SEM image in Figure 8. This hybrid aerogel showed slight increase in bulk density (0.148 g/mL) compared to native silica aerogel (0.118 g/mL) due to additional sPS chains. The skeletal density of hybrid aerogel (1.635 g/mL) was lower than that of the native silica aerogel (1.801 g/mL) due to lower skeletal density of sPS. The overall porosity of this hybrid aerogel (90.9%) is slightly lower than that of native silica aerogel (93.4%) indicating that sPS chains occupied some of the mesopores of silica aerogel.

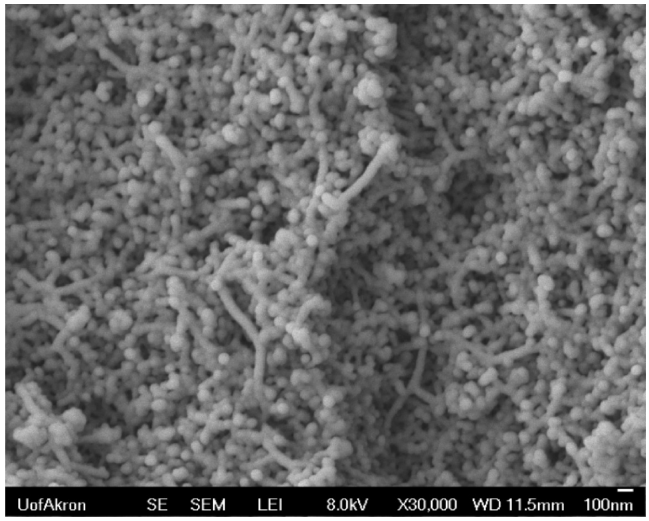

Figure 8. SEM image of Type 2 hybrid aerogel.

The compressive stress−strain curve of Type 2 hybrid aerogel is shown in Figure 9. First, the compressive modulus of

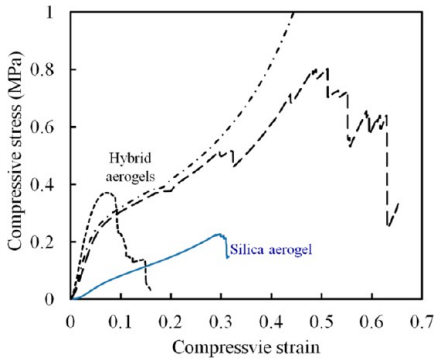

Figure 9. Stress−strain curves of three specimens of Type 2 hybrid aerogel.

the hybrid aerogel is much higher than that of silica aerogel. Second, several interruptions are seen in the stress−strain plots of two of the three specimens tested up to a compressive strain of 50%. These interruptions in the stress−strain diagram can be attributed to breakup of the silica particle networks. Such network breakup was not seen in Type 1 hybrid aerogels up to a strain of 60%. In view of this, these hybrid aerogels were not further characterized in this work.

We can now compare and contrast how the second gel networks formed in Type 1 and Type 2 hybrid aerogels. In Type 1 hybrid aerogels, the preformed sPS networks presented much larger macropores for silica networks to form easily. In addition, small molecule TEOS diffused easily in such macropores. In Type II hybrid aerogel, on the other hand, the mesopores of preformed silica gel were much more constraining against the diffusing, large molecule sPS.

4. CONCLUSIONS

In conclusion, a two-component sPS/silica hybrid aerogel was developed using a two-step synthesis method, where the silica gel network was grown in situ in the macropores of sPS gel (Type 1) or the chains of sPS were allowed to undergo diffusion and thermoreversible gelation in the mesopores of silica gel (Type 2). These hybrid aerogels combine materials with different hydrophilic nature and network morphology to obtain synergy in surface property and mechanical performance. The unique combined pore structures and mechanical synergy allowed hybrid aerogels to exhibit fast absorption and high absorption capacity for a hydrocarbon liquid. The study showed that Type 1 hybrid aerogels performed much better in terms of mechanical performance, surface area, and absorption capacity of a hydrocarbon liquid than Type 2 hybrid aerogels. We believe that other synergistic hybrid aerogel structures can be designed and fabricated following the method presented in this work.

AUTHOR INFORMATION

Corresponding Author

*E-mail: janas@uakron.edu.

Notes

The authors declare no competing financial interest.

REFERENCES

(1) Kistler, S. S. *Nature* **1931**, *127*, 741.
(2) Tewari, P. H.; Hunt, A. J.; Lofftus, K. D. *Mater. Lett.* **1985**, *3*, 363−367.
(3) Wittwer, V. *J. Non-Cryst. Solids* **1992**, *145*, 233−236.
(4) Dorcheh, A. S.; Abbasi, M. H. *J. Mater. Process. Technol.* **2008**, *199*, 10−26.
(5) Rao, A. V. *Solid State Phys.* **1999**, *41*, 14−17.
(6) Hrubesh, L. W.; Keene, L. E.; Latorre, V. R. *J. Mater. Res.* **1993**, *8*, 1736−1741.
(7) Gerlach, R.; Kraus, O.; Fricke, J.; Eccardt, P. C.; Kroemer, N.; Magori, V. *J. Non-Cryst. Solids* **1992**, *145*, 227−232.
(8) Yoldas, B. E.; Annen, M. J.; Bostaph, J. *Chem. Mater.* **2000**, *12*, 2475−2484.
(9) Akimov, Y. K. *Instrum. Exp. Tech.* **2003**, *46*, 287−299.
(10) Zhang, G.; Dass, A.; Rawashdeh, A. M.; Thomas, J.; Counsil, J. A.; Sotiriou-Leventis, C.; Fabrizio, E. F.; Ilhan, F.; Vassilaras, P.; Scheiman, D. A.; McCorkle, L.; Palczer, A.; Johnston, J. C.; Meador, M. A.; Leventis, N. *J. Non-Cryst. Solids* **2004**, *350*, 152−164.
(11) Bertino, M. F.; Hund, J. F.; Sosa, J.; Zhang, G.; Sotiriou-Leventis, C.; Leventis, N.; Tokuhiro, A. T.; Terry, J. *J. Non-Cryst. Solids* **2004**, *333*, 108−110.
(12) Kartal, A. M.; Erkey, C. J. *Supercrit. Fluids* **2010**, *53*, 115−120.
(13) Hegde, N. D.; Rao, A. V. *Appl. Surf. Sci.* **2006**, *253*, 1566−1572.
(14) Randall, J. P.; Meador, M. A. B.; Jana, S. C. *ACS Appl. Mater. Interfaces* **2011**, *3*, 613−626.
(15) Boday, D. J.; Stover, R. J.; Muriithi, B.; Keller, M. W.; Wertz, J. T.; Obrey, K. A. D.; Loy, D. A. *ACS Appl. Mater. Interfaces* **2009**, *1*, 1364−1369.
(16) Ilhan, U. F.; Fabrizio, E. F.; McCorkle, L.; Scheiman, D. A.; Dass, A.; Palczer, A.; Meador, M. A. B.; Johnston, J. C.; Leventis, N. *J. Mater. Chem.* **2006**, *16*, 3046−3054.
(17) Meador, M. A. B.; Capadona, L. A.; McCorkle, L.; Papadopoulos, D. S.; Leventis, N. *Chem. Mater.* **2007**, *19*, 2247−2260.
(18) Meador, M. A. B.; Fabrizio, E. F.; Ilhan, F.; Dass, A.; Zhang, G.; Vassilaras, P.; Johnston, J. C.; Leventis, N. *Chem. Mater.* **2005**, *17*, 1085−1098.
(19) Nguyen, B. N.; Meador, M. A. B.; Medoro, A.; Arendt, V.; Randall, J.; McCorkle, L.; Shonkwiler, B. *ACS Appl. Mater. Interfaces* **2010**, *2*, 1430−1443.
(20) Duan, Y.; Jana, S. C.; Reinsel, A. M.; Lama, B.; Espe, M. P. *Langmuir* **2012**, *28*, 15362−15371.
(21) Meador, M. A. B.; Vivod, S. L.; McCorkle, L.; Quade, D.; Sullivan, R. M.; Ghosn, L. J.; Clark, N.; Capadona, L. A. *J. Mater. Chem.* **2008**, *18*, 1843−1852.
(22) Li, L.; Yalcin, B.; Nguyen, B. N.; Meador, M. A. B.; Cakmak, M. *ACS Appl. Mater. Interfaces* **2009**, *1*, 2491−2501.
(23) Karout, A.; Buisson, P.; Perrard, A.; Pierre, A. C. *J. Sol-Gel Sci. Technol.* **2005**, *36*, 163−171.
(24) Parale, V. G.; Mahadik, D. B.; Mahadik, S. A.; Kavale, M. S.; Rao, A. V.; Wagh, P. B. *J. Sol-Gel Sci. Technol.* **2012**, *63*, 573−579.
(25) Maloney, R.; Sakamoto, J. *J. Non-Cryst. Solids* **2011**, *357*, 2059−2062.
(26) Daniel, C.; Alfano, D.; Venditto, V.; Cardea, S.; Reverchon, E.; Larobina, D.; Mensitieri, G.; Guerra, G. *Adv. Mater.* **2005**, *17*, 1515−1518.
(27) Figueroa-Gerstenmaier, S.; Daniel, C.; Milano, G.; Vitillo, J. G.; Zavorotynska, O.; Spoto, G.; Guerra, G. *Macromolecules* **2010**, *43*, 8594−8601.
(28) Figueroa-Gerstenmaier, S.; Daniel, C.; Milano, G.; Guerra, G.; Zavorotynska, O.; Vitillo, J. G.; Zecchina, A.; Spoto, G. *Phys. Chem. Chem. Phys.* **2010**, *12*, 5369−5374.
(29) Daniel, C.; Sannino, D.; Guerra, G. *Chem. Mater.* **2008**, *20*, 577−582.
(30) Wang, X.; Jana, S. C. *Polymer* **2013**, *54*, 750−759.
(31) Wu, S.. *J. Polym. Sci., Part C* **1971**, *34*, 19−30.
(32) Parvathy Rao, A.; Rao, A. V. *J. Non-Cryst. Solids* **2009**, *355*, 2260−2271.
(33) Wang, X.; Jana, S. C. *Langmuir* **2013**, *29*, 5589−5598.